A NOVEL BOUNDARY INTEGRAL METHOD FOR SLOW FREE SURFACE FLOWS

LOÏC GOBET & ROBERT G. OWENS*
Département de Mathématiques et de Statistique, Université de Montréal, Canada

ABSTRACT
The present article introduces a novel boundary integral method (BIM), adapted from an earlier method of Hansen and Kelmanson (1992, 1994) and suitable for the solution of creeping flow boundary value problems where the boundary presents singularities in the stresses. We use the new BIM to solve the problem of the planar extrusion of a Newtonian fluid at zero Reynolds number and, in particular, to determine the shape of the free surface in the immediate neighbourhood of the separation point for a range of capillary numbers. The proposed method incorporates the singular solution near the separation point, thus overcoming one limitation of a classical BIM to the problem (see, for example, Kelmanson (1983)). In a recent article, Owens (2022) also incorporated the singular solution into his BIM formulation. However, since the integration path used in the present BIM passes directly through the separation point this leads to an important improvement on the method of Owens (2022), who was obligated to skirt the singularity due to the non-integrability there of the normal derivative of the vorticity. Results presented for the extrudate swell ratio, the angle of separation and the leading exponent in the asymptotic expression for the stream function are shown to be in convincing agreement with others in the theoretical, numerical and experimental literature.
Keywords: Stokes flow, singularity, boundary integral method, free surface flows.

1 INTRODUCTION

The use of boundary integral methods (BIMs) for the solution of Poisson's equation and the biharmonic equation arising in boundary value problems in such fields as linear elasticity, electrostatics, potential flows and slow viscous flows dates back some fifty years. That such methods only require boundary data for the computation of the solution throughout the domain of definition presents both advantages and disadvantages. On the positive side, and where applicable, BIMs are, in general, more cost-efficient than other mesh-based methods, giving rise to much smaller linear systems to be solved than those arising from equivalent finite element or finite difference (FD) approximations, for example, albeit with matrices that may be ill-conditioned. However, the presence of singularities on the boundary due to a sharp corner or a sudden change of boundary condition, for example, leads to poor convergence of classical BIMs and the need to treat such singularities in a mathematically rigorous fashion has spawned a number of different techniques in the literature.

1.1 BIMs for boundary value problems with singularities on the boundary

In 1983, Kelmanson [1], [2] used a singular subtraction (SS) BIM to solve three problems: the steady lid-driven cavity problem, the problem of the slow channel flow of a viscous fluid through a sudden expansion and the planar "stick-slip" problem for a viscous fluid. The dominant asymptotic behaviour of the stream function ψ in the neighbourhood of the singularities in these problems was written down by Kelmanson in the form of truncated series g whose coefficients had to be determined as part of the solution process. Provided that

*ORCID: http://orcid.org/0000-0002-9907-2586

WIT Transactions on Engineering Sciences, Vol 135, © 2023 WIT Press
www.witpress.com, ISSN 1743-3533 (on-line)
doi:10.2495/BE460111

the truncated series had a sufficient number of terms, the recasting of the problems in terms of a modified stream function

$$\chi := \psi - g, \tag{1}$$

meant that the modified flow variables became regular throughout the flow domains. By evaluating the kernel integrals exactly rather than by Gaussian quadrature computer time savings of up to 38% were realised and, in the first of the two articles, CPU time and storage savings compared with FD methods were shown to be substantial.

The subtraction of a truncated series representation of the asymptotic behaviour at a boundary singularity of the solution to an elliptic boundary value problem has been done for boundary value problems involving harmonic functions and this dates back to the SS method of Symm [3]. Ingham and Kelmanson [4] used both a classical BIM and a BIM modified using the SS method to solve two Laplacian boundary value problems for a potential function φ. One problem (A) had Dirichlet conditions prescribed for φ where the singularity was due to a discontinuous boundary potential and the other problem (B) featured a discontinuity in the prescribed boundary flux. A comparison with FD calculations, where the finite difference boundary mesh points coincided with the BIM segment end points, showed that for finer meshes the two BIMs used considerably less CPU time for problem B. In the case of problem A, it was only the possibility of calculating an optimal relaxation parameter for the FD SOR iterations that allowed that method to require less CPU time to converge than the BIMs. The modified BIM was considerably more accurate than the classical BIM for problem A, and only required about 10% more CPU time.

In 1984, Kelmanson [5] and Ingham and Kelmanson [6] used a singularity incorporation (SI) BIM to solve nonlinear problems of two dimensional steady state heat transfer, the conducting medium having variable thermal conductivity. Under a Kirchoff transformation the transformed variable T satisfied Laplace's equation and the series representation of the behaviour of T in the neighbourhood of a boundary singularity was enforced solely on a small number of elements nearest to the singularity, in contrast to the SS method of Symm [3]. Thus the modification to the classical BIM was small although the authors reported dramatic improvements in the rate of convergence of results throughout the solution domain of the problems considered.

Where applicable, the so-called singularity annihilation (SA) BIM, employed by Kelmanson and Lonsdale [7], has the advantage over both SS and SI BIMs in that it requires no extra coding and employs the natural boundary conditions of the original problem. The basic idea is a simple one: if the boundary singularities are in a region of the boundary where suitably constructed Green's functions are asymptotically small then the solution's singular behaviour may be annihilated. This was achieved by the authors for the benchmark lid-driven cavity problem where the asymptotic behaviour $\psi = \mathcal{O}(r)$ of the stream function ψ in corners between the moving lid and the vertical walls is the same as that of Taylor's scraper flow problem [8] and leads to $\mathcal{O}(r^{-1})$ behaviour of the vorticity and pressure at these points: a particularly severe test of the numerical method. Comparisons of the calculated stream function values with those obtained using the SS method of Kelmanson [1] showed impressive agreement and were corroborated by the biharmonic method of fundamental solutions of Karageorghis and Fairweather [9]. However, the SA BIM required substantially less coding than the SS BIM of Kelmanson [1].

The $\mathcal{O}(r^{-1})$ behaviour of the stresses at the singular points between the lid and walls in the lid-driven cavity problem mean that they are not integrable and that therefore it is not a physically realizable flow. Hansen and Kelmanson [10], [11] used a BIM to investigate the effect of introducing small leaks at the corners where the lid meets the walls, thus making the flow physical and modelling what must take place under experimental conditions. Near

the re-entrant corners in the leaky lid-driven cavity problem the authors showed that the stream function $\psi = \mathcal{O}(r^{1+\lambda})$ with λ real and in the interval $(0, 1)$. Thus, the vorticity ω and pressure p were now integrable but the normal derivative of the vorticity $\partial\omega/\partial n$, appearing in the integral formulae for ψ and ω, was not. However, the authors were able to evaluate these integrals without avoiding the re-entrant corner by noting that on a piecewise smooth boundary in Stokes flow the tangential derivative of the pressure equals $\partial\omega/\partial n$ (where these exist) and that with a change of variables and integration by parts the integrals in the integral formulae were finite. The resulting BIM was first used by Xu [12].

Some 65 years ago, Michael [13] showed for the problem of creeping planar flow of a Newtonian fluid extruding from a channel that, with the assumption of either vanishing surface tension or zero curvature of the free surface near the separation point, the angle formed between the free surface and the channel wall was $180°$. Since that time there has been widespread disagreement, both in the experimental and numerical literature, about the character of the free surface (and therefore about the solution to the problem) in the neighbourhood of the channel orifice and, in particular, about the angle of separation. The values of the separation angles computed by Owens [14] for capillary numbers Ca ranging from 1 to 1,000 fell well within the interval of values published in previous experimental and numerical papers, although there is a paucity of such results available in the literature. His analysis showed that for non-zero surface tensions the normal stress and curvature of the free surface were unbounded at the point of separation, consistent with the analysis and results of Anderson and Davis [15], Schultz and Gervasio [16] and Salamon et al. [17]. It was concluded by Owens that the case of zero surface tension ($Ca = \infty$, with corresponding separation angle of $180°$), is a singular limit.

The problem of the planar extrusion of a Newtonian fluid at vanishing Reynolds number Re was considered by Kelmanson [18] using a classical BIM but no account of the singularity in the stresses at the separation point C was taken, leading to the author's admission that it was to be expected that near this point the numerical results would be in error. Owens [14] has also used a BIM to solve the same problem, with the incorporation of the singular solution near the separation point. However, due to the non-integrability at C of $\partial\omega/\partial n$, appearing in the integral formulae for ψ and ω, he chose a boundary integration path that closely skirted the singular point, thus introducing a source of error.

Because the shape of the free surface must be found from some iterative process and is typically non-trivial, SA BIMs are unusable for creeping planar extrusion flows with $0 < Ca < \infty$. It is not possible for these flows to employ SS BIMs either: the angle of separation being unknown a priori means that the exponents in the leading order asymptotic form g (see (1)) must be numerically calculated and it is not known how to do this for more than the first two exponents, meaning that the flow variables will not have the required regularity throughout the flow domain. In this article, we use a novel SI BIM, a modification of the BIM of Hansen and Kelmanson [10], [11], to solve the problem of the planar extrusion of a Newtonian fluid at vanishing Reynolds number Re and, in particular, to determine the shape of the free surface in the immediate neighbourhood of the separation point C for a range of capillary numbers.

The relevance of the results of our calculations to steady extrusion flows at non-zero Reynolds numbers, may be understood from the following argument of Moffatt [8]: Let us suppose that in the neighbourhood of C the stream function for the two-dimensional Navier–Stokes equations may be written in terms of local polar coordinates (r, θ) in the form

$$\psi \sim Ar^{1+\lambda} f(\theta), \tag{2}$$

for some constant A, exponent λ and function f. Then, denoting the fluid velocity by $\boldsymbol{v}$ we see that the inertial term $\boldsymbol{v} \cdot \nabla \boldsymbol{v} = \mathcal{O}(A^2 r^{2\lambda-1})$ is negligible compared to the viscous term $\nu \nabla^2 \boldsymbol{v} = \mathcal{O}(\nu A r^{\lambda-2})$ if

$$\frac{A r^{\lambda+1}}{\nu} \ll 1. \tag{3}$$

The inequality (3) holds (provided $Re(\lambda) > 0$) for r sufficiently small. That is, in the neighbourhood of the singularity we expect the behaviour to be Stokesian. Neither is the local analysis near the separation point C in the present study limited to the strictly planar case. At zero Reynolds numbers, and in the absence of gravity, the (three-dimensional) flow of a Newtonian fluid extruded from a circular die will be axisymmetric and sufficiently far from the die lip there are obvious differences between the three-dimensional and planar extrudate. Such differences would include the values of the extrudate swell ratios computed under different flow conditions [19]. Ramalingam [20] points out, however, that the analysis of the singular behaviour of the flow variables near the orifice of an axisymmetric extrusion flow may be expected to show it to be locally planar. See too an analysis of Burda [21] of the asymptotics near corners in axisymmetric Stokes flow. The novel SI BIM presented in the present article could therefore, we believe, be adapted to the axisymmetric case.

1.2 Outline

The outline of this article is as follows: After briefly presenting the governing equations for Stokes flow in Section 2.1 we proceed to give a concise mathematical description of the problem to be solved, together with the boundary conditions that apply in Section 2.2. In Section 2.3 we describe how the mathematical equation of the free surface is divided into two parts and how the two surfaces are matched at some small distance from the separation point. The form of the surface near the separation point C has slope $\tan(\alpha)$ (for an angle α which must be calculated) and allows for the possibility of infinite curvature there. Further from C we use a linear combination of linearly independent functions proposed by Kelmanson [2] whose parameters must be adjusted in an attempt to satisfy the normal force balance condition on the free surface.

In Section 2.4, and inspired by Michael [13] and Lugt and Schwiderski [22], we derive the singular form of the stream function ψ, the vorticity ω and the pressure p in the neighbourhood of the separation point. It may be concluded that the integrals representing ψ and ω in the classical BIM diverge if the integration path passes through the separation point because of the non-integrability of $\partial\omega/\partial n$ there.

In Section 3 we outline two different BIMs for the solution of the boundary value problem of interest and explain how they differ. In Section 3.1 the BIM of Hansen and Kelmanson [10], [11], already mentioned in the Introduction, is treated to a more thorough exposition. Then, in Section 3.2 we show that it is not necessary to use integration by parts on the entire boundary when $\partial\omega/\partial n$ is replaced by $\partial p/\partial s$ in the integral representations of ψ and ω, but that it may be confined to the intersection of the boundary with a small neighbourhood of the separation point. Since the integration path used in the present BIM passes directly through the separation point this is an important difference between the new method and that of Owens [14] who was obligated to skirt the singularity. In supplying details of the discretization of the new BIM in Section 3.2.1 it becomes clear that there may be fewer jump terms in the pressure to contend with than in Hansen and Kelmanson's BIM and that the boundary grid for the computation of p and the other flow variables becomes a staggered one. We enumerate some of the other advantages of the present method with respect to that of Hansen and Kelmanson in Section 3.2.2.

The parameters appearing in the linear combination of functions proposed by Kelmanson [2] for the representation of the free surface sufficiently far from the separation point are calculated using the Levenberg–Marquardt [23], [24] method which solves the non-linear least-squares problem arising from the minimisation of the residual of the normal stress balance at certain selected points on the free surface. We explain this is more detail in Section 3.3.

Some numerical results, obtained on three different meshes, are presented in Section 4. It is shown in Section 4.1 that for any given surface tension, the (positive) slope of the free surface attains a maximum near the separation point and that the second derivative grows dramatically as the separation point is approached along the free surface, the curvature at the separation point itself being infinite. In Section 4.2 we present results for the extrudate swell ratio over a range of capillary numbers and these are shown to be in excellent agreement with others in the numerical literature [14], [17], [19], [25]. However, recognising that the extrudate swell ratio is a somewhat crude measure of the correctness of the solution, in Section 4.3 we also post our calculated values for the separation angles α and leading order indices λ_1 appearing in the asymptotic forms of the flow variables in the immediate neighbourhood of the separation point. The dearth and spread of data for these two parameters in the scientific literature, be it theoretical [16], numerical [17] or experimental [26]–[29] make comparisons difficult although agreement between our results with what has been previously published would seem to be satisfactory.

2 PLANAR EXTRUSION OF A NEWTONIAN FLUID AT VANISHING REYNOLDS NUMBER

2.1 Governing equations for steady planar Stokes flow

The governing non-dimensional equations for steady Stokes flow in a domain Ω are

$$\nabla \cdot \boldsymbol{v} = 0, \qquad \text{in } \Omega, \tag{4}$$

$$-\nabla p + \Delta \boldsymbol{v} = \boldsymbol{0}, \qquad \text{in } \Omega, \tag{5}$$

where $\boldsymbol{v}$ is the fluid velocity and p is the pressure. In two dimensions, (4) allows us to introduce a stream function ψ such that $\boldsymbol{v} = (u(x,y), v(x,y))$ may be written

$$\boldsymbol{v} = \nabla \times (0,0,\psi) \Rightarrow u = \frac{\partial \psi}{\partial y} \text{ and } v = -\frac{\partial \psi}{\partial x}, \tag{6}$$

where, in the usual notation, x and y are dimensionless Cartesian coordinates. By calculating the curl of (5) we get the biharmonic equation for ψ:

$$\Delta^2 \psi = 0. \tag{7}$$

We now introduce $\omega := \Delta\psi$, and see that (7) may be re-expressed as a system of coupled equations

$$\begin{cases} \Delta\omega = 0, & \text{in } \Omega, \\ \Delta\psi = \omega, & \text{in } \Omega. \end{cases} \tag{8}$$

2.2 Geometry, problem description and boundary conditions

2.2.1 Problem geometry and assumptions

The upper portion of the two-dimensional geometry of the problem to be solved is shown in Fig. 1. Dimensionless Cartesian coordinates (x, y) are used and x is chosen, in a natural way,

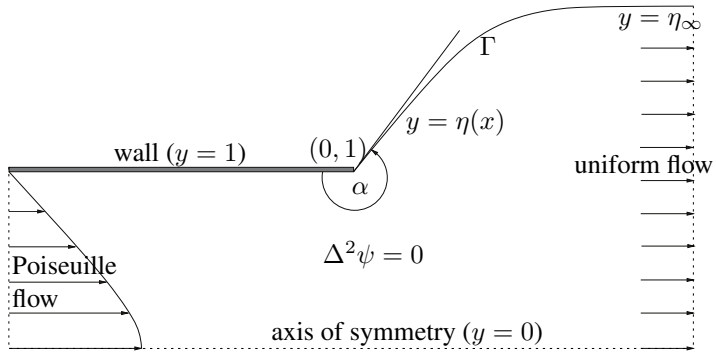

Figure 1: Problem geometry of planar extrusion.

as the stream-wise coordinate. Far upstream a Newtonian fluid is driven, at negligibly small Reynolds number, by a constant dimensionless pressure gradient $\partial p/\partial x$ along the channel formed between two parallel walls $y = \pm 1$ giving rise to steady planar Poiseuille flow. At $x = 0$ the fluid is extruded into air and the points $(0, \pm 1)$ are separation points where the fluid undergoes a transition from being confined by the walls to forming a jet. The tangent to the free surface Γ at the point of separation $(0, 1)$ forms an angle α with the solid wall $y = 1$, as shown in Fig. 1. Sufficiently far downstream of the line of extrusion into air the flow is considered to be steady and uniform and the free surface is parallel to the $x-$axis, having equation $y = \eta_\infty$ for some constant η_∞, called the extrudate swell ratio.

2.2.2 Boundary conditions for ψ and ω

The coupled eqn (8) are solved subject to boundary conditions derived by further assuming no-slip and no-penetration conditions along the solid wall $\{x \leq 0,\ y = 1\}$, unit volume flow rate in the upper half channel far upstream, and zero shear and normal stresses along the free surface Γ and axis of symmetry $y = 0$.

At entry ($x \to -\infty$) we have

$$\psi = \frac{3}{2} y \left(1 - \frac{y^2}{3}\right),\ \omega = -3y, \tag{9}$$

whereas at exit ($x \to \infty$) uniform flow and incompressibility lead to

$$\psi = \frac{y}{\eta_\infty},\ \omega = 0. \tag{10}$$

No-slip and no-penetration conditions on the upper solid wall $\{x \leq 0,\ y = 1\}$ are ensured by prescribing

$$\psi = 1,\ \frac{\partial \psi}{\partial y} = 0, \tag{11}$$

and along the axis of symmetry ($y = 0$) the zero shear-rate and no-penetration conditions give rise to

$$\psi = 0,\ \frac{\partial^2 \psi}{\partial y^2} = 0. \tag{12}$$

Along the free surface Γ, continuous with the solid wall, we must now have

$$\psi = 1. \tag{13}$$

Let $\partial^2/\partial t^2$ denote the second-order tangential derivative. Then, the zero shear-stress condition on the free surface

$$\frac{\partial^2 \psi}{\partial n^2} - \frac{\partial^2 \psi}{\partial t^2} = 0, \tag{14}$$

can be used to show (see, for example, Batchelor [30] or Longuet-Higgins [31]) that on Γ

$$\omega = -2\kappa \frac{\partial \psi}{\partial n}, \tag{15}$$

where κ is the signed curvature, defined by

$$\kappa = -\nabla \cdot \hat{\boldsymbol{n}}, \tag{16}$$

and $\hat{\boldsymbol{n}}$ is the unit outward pointing normal vector on Γ. Finally, a normal force balance on the free surface gives

$$[p] + 2\frac{\partial^2 \psi}{\partial n \partial s} + \gamma\kappa = 0, \tag{17}$$

where the excess pressure $[p] := p - p_a$ is the difference between the fluid pressure p and atmospheric pressure p_a, γ is the surface tension and $\partial/\partial s$ $(= \partial/\partial t)$ denotes a derivative with respect to arc length along Γ. From this point on, and to ease the notation, we will simply denote the excess pressure by p.

2.3 Mathematical description of the free surface

The mathematical equation of the free surface Γ is divided into two parts and the two surfaces are matched at some small distance $r_c > 0$ from the separation point C. The free surface at the separation point has slope $\tan(\alpha)$ and we allow for the possibility of infinite curvature there. Further from C we use a linear combination of linearly independent functions proposed by Kelmanson [2] whose parameters must be adjusted in an attempt to satisfy the normal force balance condition (17).

2.3.1 At a distance $r \geq r_c$ from the separation point C

Sufficiently far from the separation point the equation of the free surface Γ is written $y = \eta(x)$, where

$$\eta(x) = \sum_{i=1}^{n} \beta_i \, \eta_i(x), \tag{18}$$

and where the n linearly independent functions $\{\eta_i\}_{i=1}^n$ are defined by

$$\eta_i(x) = 1 + \alpha_i \, \tanh\left(x\left(\varepsilon_{\infty,i} - (\varepsilon_{0,i} - \varepsilon_{\infty,i})\exp(-\gamma_i\, x)\right)\right), \qquad i = 1, 2, \ldots, n. \tag{19}$$

The parameters $\{\alpha_i, \varepsilon_{\infty,i}, \varepsilon_{0,i}, \gamma_i\}$ appearing in (19), together with the $\{\beta_i\}_{i=1}^n$ of (18) are to be determined. Although the form (18) is not used at C we nevertheless impose $\eta(0) = 1$. This constraint means that

$$\sum_{i=1}^{n} \beta_i = 1, \tag{20}$$

which reduces the number of parameters in (18) that need to be calculated to $5n - 1$.

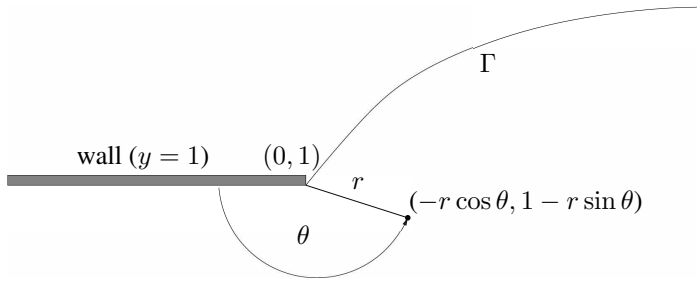

Figure 2: Polar angle θ measured in the anti-clockwise direction from the channel wall $y = 1$.

2.3.2 At a distance $r \leq r_c$ from the separation point C

In the sector centred at C and of radius r_c we express the equation of the free surface in polar coordinates (again, see Fig. 2) as the truncated series

$$y = 1 + h(r) = 1 - r\,\sin\alpha + h_1\,r^{\lambda_1+1} + h_2\,r^{2\lambda_1+1} - \frac{c_p\,r^2}{2\gamma}\cos\alpha, \tag{21}$$

where the parameters $\{\alpha, \lambda_1, h_1, h_2, c_p\}$ are found so that to leading orders the curve Γ and its curvature might be continuous at $r = r_c$, so that non-trivial singular solutions (see Section 2.4) may be found for all variables in the sector of radius r_c centred at C and so that to leading orders the normal stress balance (17) may be satisfied on the surface (21).

2.4 Singular representations

We now seek a solution to the biharmonic equation (7) in the near neighbourhood of the separation point. One can show (see, for example, Michael [13] or Lugt and Schwiderski [22]) that in a sector centred at $(0, 1)$ and provided that $\lambda_n \neq 1$ and $Re(\lambda_n) > 0$ $(n = 1, 2, \ldots)$, ψ may be written in the form

$$\psi = 1 + \sum_{n=1}^{\infty} r^{\lambda_n+1} f_n(\theta), \tag{22}$$

where r and θ are polar coordinates centred at $(0, 1)$ (see Fig. 2), the eigenvalues λ_n are to be determined and

$$f_n(\theta) = A_n \cos\left((\lambda_n + 1)\theta\right) + B_n \sin\left((\lambda_n + 1)\theta\right) + C_n \cos\left((\lambda_n - 1)\theta\right) + D_n \sin\left((\lambda_n - 1)\theta\right), \tag{23}$$

where $\{A_n, B_n, C_n, D_n\}$ $(n = 1, 2, 3, \ldots)$ are coefficients to be calculated. The radial and transverse components of the velocity $\boldsymbol{v}$ are given by

$$v_r = \frac{1}{r}\frac{\partial\psi}{\partial\theta} = \sum_{n=1}^{\infty} r^{\lambda_n} f_n'(\theta) \text{ and } v_\theta = -\frac{\partial\psi}{\partial r} = -\sum_{n=1}^{\infty}(\lambda_n + 1) r^{\lambda_n} f_n(\theta), \tag{24}$$

so that, as observed for example by Sturges [32], the weak regularity condition $Re(\lambda_n) > 0$ means that the velocity vanishes as $r \to 0$. Following Michael [13], we also observe that

$Re(\lambda_n) > 0$ is a physical requirement in order that the integrated stresses remain finite as $r \to 0$.

The boundary conditions (11), (13) and (14) may be shown to give rise to a homogeneous linear system of equations for A_1, B_1, C_1 and D_1 which, provided that it is singular, allows the determination of three of these coefficients in terms of the fourth. In the present paper we choose to find A_1, B_1 and D_1 in terms of C_1. The boundary conditions of Section 2.2.2 also allow A_2, B_2, C_2 and D_2 to be written in terms of C_1. In agreement with the r exponent in the correction $Ca\psi_1$ to the leading order term in the perturbation expansion (2.13a) of the stream function in an article of Anderson and Davis [15], it may be shown [14] that $\lambda_2 = 2\lambda_1$ is necessary in order that the separation angle α be different from π. Thus, for $i = 1, 2$ we may write

$$f_i(\theta) = C_1 F_i(\theta), \qquad i = 1, 2,$$

with the function F_i having as parameters only λ_1 and α. Truncating (22) after two terms we are therefore left with

$$\psi(r, \theta) \sim 1 + C_1 \Psi(r, \theta), \tag{25}$$

where we define

$$\Psi(r, \theta) := r^{\lambda_1 + 1} F_1(\theta) + r^{2\lambda_1 + 1} F_2(\theta). \tag{26}$$

A singular expression for p in the neighbourhood of the separation point may be obtained using (5) and the relationship (6) between $\boldsymbol{v}$ and ψ:

$$p \sim C_1 \Pi(r, \theta) - c_p, \tag{27}$$

where

$$\Pi(r, \theta) := \frac{r^{\lambda_1 - 1}}{\lambda_1 - 1}((\lambda_1 + 1)^2 F_1'(\theta) + F_1^{(3)}(\theta)) + \frac{r^{2\lambda_1 - 1}}{2\lambda_1 - 1}((2\lambda_1 + 1)^2 F_2'(\theta) + F_2^{(3)}(\theta)), \tag{28}$$

and c_p is a constant in the definition of $y = 1 + h(r)$ (see eqn (21)).

Finally, using $\omega = \Delta\psi$ (see (8)) we get an expression for ω in the neighbourhood of the separation point:

$$\omega(r, \theta) \sim C_1 \Omega(r, \theta), \tag{29}$$

where

$$\Omega(r, \theta) := (1 + \lambda_1)^2 \, r^{\lambda_1 - 1} F_1(\theta) + (1 + 2\lambda_1)^2 \, r^{2\lambda_1 - 1} F_2(\theta). \tag{30}$$

The coefficient C_1 in (25), (27) and (29) is to be determined. λ_1 and α appearing in the functions F_1 and F_2 and c_p a constant in (27) are found from a nonlinear least-squares calculation of the free surface, as will be described in Section 3.3. One can show (see, for example, Table 1 of Sturges [32]) that if $\alpha \in [\pi, 3\pi/2]$ the value of λ_1 will be real and remain in the interval $[1/3, 1/2]$. Therefore, from (26), (28) and (30) whereas ψ, $\partial\psi/\partial n$, p and ω are all Riemann integrable at $r = 0$, $\partial\omega/\partial n = \mathcal{O}(r^{\lambda_1 - 2})$ is not.

3 BOUNDARY INTEGRAL FORMULATIONS FOR THE SOLUTION OF (7)

Let Ω be the truncated domain whose boundary $\partial\Omega$ is $AB \cup BC' \cup C'C_\rho' \cup \mathscr{C}_\rho \cup C_\rho'' C'' \cup C''D \cup DE \cup EA$, as shown in Figs 3 and 4. The inflow boundary AB is set at a finite distance $-x_{-\infty}$ upstream and the outflow boundary DE a finite distance x_∞ downstream of the die exit. C is the separation point $(0, 1)$ and the points C' and C'' are both at a distance r_c from C on the wall BC and the free surface CD, respectively. Thus, C' is the point $(-r_c, 1)$

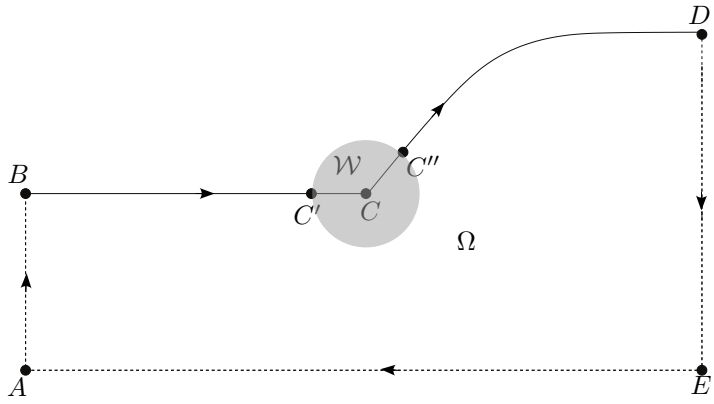

Figure 3: The truncated flow domain $ABCDE$ and the singular region $\mathcal{W} \cap \overline{\Omega}$..

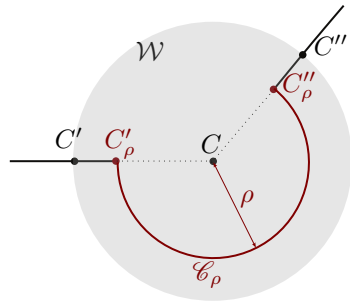

Figure 4: Figure showing the integration path $C'C'_\rho \cup \mathscr{C}_\rho \cup C''_\rho C''$ contained in the singular region $\mathcal{W} \cap \overline{\Omega}$.

and C'' the point $(x_0, \eta(x_0))$ where x_0 is the positive root of

$$x_0^2 + (\eta(x_0) - 1)^2 = r_c^2. \tag{31}$$

In Figs 3 and 4, the points C'_ρ and C''_ρ are points on the wall BC and the free surface CD, respectively, a distance $0 < \rho \leq r_c$ from C. $\mathscr{C}_\rho$ is the arc of radius ρ centred at C, having initial point C'_ρ and end point C''_ρ, as shown in Fig. 4. $\mathcal{W}$ denotes the disk of radius r_c centred at C and in the sector $\mathcal{W} \cap \overline{\Omega}$ the singular forms (25), (27) and (29) or their derivatives will be used to represent all flow variables appearing in (32), (33) and (39).

Suppose that $P(x', y')$ is an arbitrary point in $\mathbb{R}^2$. Then, using Green's identities it can be shown that $\psi(x', y')$ and $\omega(x', y')$, the solutions to (8), may be expressed in integral form as

$$\xi(x', y')\omega(x', y') = \int_{\partial\Omega} \left(\frac{\partial \omega}{\partial n} G_1 - \omega \frac{\partial G_1}{\partial n} \right) \, ds, \tag{32}$$

$$\xi(x', y')\psi(x', y') = \int_{\partial\Omega} \left(\frac{\partial \omega}{\partial n} G_2 - \omega \frac{\partial G_2}{\partial n} + \frac{\partial \psi}{\partial n} G_1 - \psi \frac{\partial G_1}{\partial n} \right) \, ds, \tag{33}$$

where the normal derivative $\partial/\partial n := \hat{\boldsymbol{n}} \cdot \nabla$ and $\hat{\boldsymbol{n}}$ is an outward pointing unit normal vector to $\partial\Omega$. The factor $\xi(x', y')$ in (32) and (33) is defined by

$$\xi(P) = \begin{cases} \dfrac{\varphi}{2\pi} & \text{if } P \in \partial\Omega, \\ 1 & \text{if } P \in \Omega, \\ 0 & \text{otherwise}, \end{cases} \tag{34}$$

where φ is the angle between the left and right tangents at the boundary point P when $P \in \partial\Omega$. The functions $G_1 = G_1(x, y, x', y')$ and $G_2 = G_2(x, y, x', y')$ appearing in (32) and (33) are fundamental solutions of, respectively, the two-dimensional Laplace's equation and biharmonic equation, chosen to be

$$G_1 = -\frac{1}{4\pi}\log((x-x')^2 + (y-y')^2), \tag{35}$$

$$G_2 = -\frac{1}{16\pi}(((x-x')^2 + (y-y')^2)(\log((x-x')^2 + (y-y')^2) - 2)). \tag{36}$$

Along a plane piecewise smooth curve $\mathcal{C}$ it may be easily shown from (5) and (6) that

$$\frac{\partial p}{\partial s} = \frac{\partial \omega}{\partial n}, \tag{37}$$

almost everywhere, a result that will be seen to be of central importance in the sections that follow.

3.1 The formulation of Hansen and Kelmanson [10], [11]

The approach of Hansen and Kelmanson [10], [11] uses integration by parts to write, along a smooth finite curve $\mathcal{C}$ having initial point a and end point b

$$\int_{\mathcal{C}} \frac{\partial \omega}{\partial n} G \, ds = \int_{\mathcal{C}} \frac{\partial p}{\partial s} G \, ds = pG(b) - pG(a) - \int_{\mathcal{C}} p \frac{\partial G}{\partial s} \, ds, \tag{38}$$

where G is some suitable differentiable function and it has been assumed that pG is continuous along $\mathcal{C}$. Setting $G = G_1$ (35) or G_2 (36), the generalization of (38) to the simple closed piecewise smooth boundary curve $\mathcal{C} = \partial\Omega$, where pG has a finite number of jumps, is straightforward and, in the present case, leads to

$$\begin{aligned}
&\int_{\partial\Omega} \frac{\partial p}{\partial s} G_j \, ds = \int_B^{C'_\rho} \frac{\partial p}{\partial s} G_j \, ds + \int_{\mathscr{C}_\rho} \frac{\partial p}{\partial s} G_j \, ds + \int_{C''_\rho}^{D} \frac{\partial p}{\partial s} G_j \, ds + \int_E^A \frac{\partial p}{\partial s} G_j \, ds \\
&= [pG_j]_B^{C'-} + [pG_j]_{C'+}^{C'_\rho} + [pG_j]_{C''_\rho}^{C''_\rho} + [pG_j]_{C''_\rho}^{C''-} + [pG_j]_{C''+}^{D} + [pG_j]_E^A \\
&- \int_B^{C'_\rho} p\frac{\partial G_j}{\partial s} \, ds - \int_{\mathscr{C}_\rho} p\frac{\partial G_j}{\partial s} \, ds - \int_{C''_\rho}^{D} p\frac{\partial G_j}{\partial s} \, ds - \int_E^A p\frac{\partial G_j}{\partial s} \, ds \\
&= -[pG_j]_A^B - [pG_j]_{C'-}^{C'+} - [pG_j]_{C''-}^{C''+} - \int_B^{C'_\rho} p\frac{\partial G_j}{\partial s} \, ds - \int_{\mathscr{C}_\rho} p\frac{\partial G_j}{\partial s} \, ds \\
&\qquad - \int_{C''_\rho}^{D} p\frac{\partial G_j}{\partial s} \, ds - \int_E^A p\frac{\partial G_j}{\partial s} \, ds, \; j = 1, 2.
\end{aligned} \tag{39}$$

We assume here and henceforth that (x', y') is not chosen to coincide with the separation point. Thus, by the integrability of $p\partial G_j/\partial s$ along $\mathscr{C}_\rho$ for all $\rho > 0$ we have, in the limit $\rho \to 0$,

$$\int_{\partial\Omega} \frac{\partial p}{\partial s} G_j \, ds = -[pG_j]_A^B - [pG_j]_{C'-}^{C'+} - [pG_j]_{C''-}^{C''+} - \int_B^D p\frac{\partial G_j}{\partial s} \, ds - \int_E^A p\frac{\partial G_j}{\partial s} \, ds, \tag{40}$$

where it is understood (since $C'_\rho, C''_\rho \to C$ when $\rho \to 0$) that

$$\int_B^D p\frac{\partial G_j}{\partial s} \, ds = \int_B^{C'} p\frac{\partial G_j}{\partial s} \, ds + \int_{C'}^C p\frac{\partial G_j}{\partial s} \, ds + \int_C^{C''} p\frac{\partial G_j}{\partial s} \, ds + \int_{C''}^D p\frac{\partial G_j}{\partial s} \, ds. \tag{41}$$

Thus, (40) becomes

$$\int_{\partial\Omega} \frac{\partial p}{\partial s} G_j \, ds = -[pG_j]_A^B - [pG_j]_{C'-}^{C'+} - [pG_j]_{C''-}^{C''+} - \int_B^{C'} p\frac{\partial G_j}{\partial s} \, ds - \int_{C'}^C p\frac{\partial G_j}{\partial s} \, ds - \int_C^{C''} p\frac{\partial G_j}{\partial s} \, ds - \int_{C''}^D p\frac{\partial G_j}{\partial s} \, ds - \int_E^A p\frac{\partial G_j}{\partial s} \, ds. \tag{42}$$

In [10], [11], Hansen and Kelmanson's boundary integral discretizations of eqns (32) and (33) used midpoint collocation for the pressure and vorticity in each of the subintervals outside a singular region.

3.2 A new formulation

Rather than perform an integration by parts all along $\partial\Omega$, as in (38), we propose to do so only along that part of $\partial\Omega$ that is within $\mathcal{W} \cap \overline{\Omega}$ (where all variables have a singular representation) and then let $\rho \to 0$. (Of course, another possibility would be to retain $\partial\omega/\partial n G_j$ $(j = 1, 2)$ outside $\mathcal{W} \cap \overline{\Omega}$ but then if the pressure is subsequently needed on the boundary it will have to be determined in a post-processing step by integrating (37) along $\partial\Omega$.) First of all,

$$\int_{\partial\Omega} \frac{\partial p}{\partial s} G_j \, ds = \int_B^{C'} \frac{\partial p}{\partial s} G_j \, ds + \left(\int_{C'}^{C'_\rho} \frac{\partial p}{\partial s} G_j \, ds + \int_{\mathscr{C}_\rho} \frac{\partial p}{\partial s} G_j \, ds + \int_{C''_\rho}^{C''} \frac{\partial p}{\partial s} G_j \, ds \right) + \int_{C''}^D \frac{\partial p}{\partial s} G_j \, ds + \int_E^A \frac{\partial p}{\partial s} G_j \, ds. \tag{43}$$

We now use integration by parts on the terms inside the parentheses in (43) and then let $\rho \to 0$ to get

$$\begin{aligned} &\lim_{\rho\to 0} \left(\Big[p\, G_j\Big]_{C'}^{C'_\rho} + \Big[p\, G_j\Big]_{C'_\rho}^{C''_\rho} + \Big[p\, G_j\Big]_{C''_\rho}^{C''} - \int_{C'}^{C'_\rho} p\, \frac{\partial G_j}{\partial s} \, ds - \int_{\mathscr{C}_\rho} p\, \frac{\partial G_j}{\partial s} \, ds - \int_{C''_\rho}^{C''} p\, \frac{\partial G_j}{\partial s} \, ds \right) \\ &= \lim_{\rho\to 0} \left(p\, G_j(C''-) - p\, G_j(C'+) - \int_{C'}^{C'_\rho} p\, \tfrac{\partial G_j}{\partial s} \, ds - \int_{\mathscr{C}_\rho} p\, \tfrac{\partial G_j}{\partial s} \, ds - \int_{C''_\rho}^{C''} p\, \tfrac{\partial G_j}{\partial s} \, ds \right) \\ &= [p\, G_j]_{C'+}^{C''-} - \int_{C'}^C p\, \tfrac{\partial G_j}{\partial s} \, ds - \int_C^{C''} p\, \tfrac{\partial G_j}{\partial s} \, ds, \end{aligned} \tag{44}$$

where, again, $(x', y') \neq (0, 1)$ and the integrability of $p\partial G_j/\partial s$ along $\mathscr{C}_\rho$ for all $\rho > 0$ has allowed us to write

$$\lim_{\rho\to 0} \int_{\mathscr{C}_\rho} p\, \frac{\partial G_j}{\partial s} \, ds = 0.$$

In summary, (43) becomes

$$\int_{\partial\Omega} \frac{\partial p}{\partial s} G_j \, ds = \Big[p \, G_j \Big]_{C'+}^{C''-} + \int_B^{C'} \frac{\partial p}{\partial s} G_j \, ds - \int_{C'}^{C} p \, \frac{\partial G_j}{\partial s} \, ds - \int_{C}^{C''} p \, \frac{\partial G_j}{\partial s} \, ds + \int_{C''}^{D} \frac{\partial p}{\partial s} G_j \, ds + \int_E^A \frac{\partial p}{\partial s} G_j \, ds. \quad (45)$$

3.2.1 Discretization

Referring throughout this section to Fig. 5, we now discretize the integrals appearing on the right-hand sides of eqns (32) and (33) where, in each case, the terms involving the integrals of $\partial\omega/\partial n$ are transformed into integrals involving the pressure p, as described in eqns (43)–(45). First of all, using the boundary conditions (9) and (10) and the assumption that the flow at both entry and exit is fully developed (so that, for example, $\partial p/\partial s = 0$) we are able to evaluate the contributions along AB and DE to the integrals in (32) and (33) exactly. Then, exploiting the boundary conditions (11), (12), (13) and (15) reduces the flow variables to be determined on the boundary to just p and ω along BC and to p and $\partial\psi/\partial n$ along $CD \cup EA$ as shown in Fig. 5. Since $\partial\psi/\partial n = 0$ on the solid wall the third term in the contribution along BC to the integral on the right-hand side of (33) vanishes. Further simplification follows from the knowledge of ψ along the upper and lower boundaries. In the remainder of this section we detail the discretization of the right-hand side of (33). The treatment of the integral in (32) is analogous.

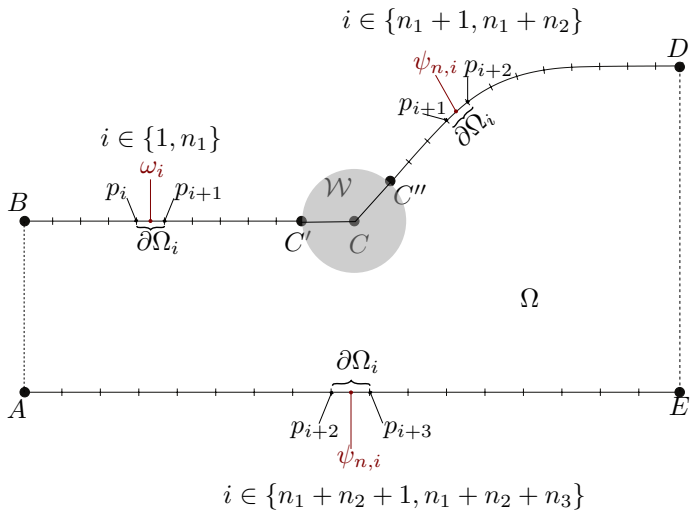

Figure 5: Summary of discrete variables along the boundary $\partial\Omega$, showing the division into $n_1 + n_2 + n_3$ sub-intervals $\partial\Omega_i$.

Along BC' The part BC' of the boundary is written as the union of n_1 subintervals $\partial\Omega_i$, $(i = 1, 2, \ldots, n_1)$ the length of the ith subinterval being denoted $\Delta x_i > 0$:

$$BC' = \bigcup_{i=1}^{n_1} \partial\Omega_i, \text{ with } |BC'| = \sum_{i=1}^{n_1} \Delta x_i. \tag{46}$$

The contribution along BC' to the integral on the right-hand side of (33) therefore becomes

$$\int_B^{C'} \left(\frac{\partial p}{\partial s} G_2 - \omega \frac{\partial G_2}{\partial n} - \frac{\partial G_1}{\partial n} \right) ds = \sum_{i=1}^{n_1} \int_{\partial\Omega_i} \left(\frac{\partial p}{\partial s} G_2 - \omega \frac{\partial G_2}{\partial n} - \frac{\partial G_1}{\partial n} \right) ds, \tag{47}$$

and on each subinterval $\partial\Omega_i$ we approximate the integral by the midpoint rule

$$\int\limits_{\partial\Omega_i} \left(\frac{\partial p}{\partial s} G_2 - \omega \frac{\partial G_2}{\partial n} - \frac{\partial G_1}{\partial n} \right) ds \approx \left(\frac{\partial p}{\partial s} \right)_i \int\limits_{\partial\Omega_i} G_2 \, ds \; - \omega_i \int\limits_{\partial\Omega_i} \frac{\partial G_2}{\partial n} \, ds \; - \int\limits_{\partial\Omega_i} \frac{\partial G_1}{\partial n} \, ds, \tag{48}$$

where $(\partial p/\partial s)_i$ and ω_i are approximations to the values of $\partial p/\partial s$ and ω at the midpoint of $\partial\Omega_i$. The partial derivative $(\partial p/\partial s)_i$ is approximated using a central difference approximation:

$$\left(\frac{\partial p}{\partial s} \right)_i \approx \frac{p_{i+1} - p_i}{\Delta x_i}, \tag{49}$$

where p_{i+1} and p_i are approximations to p at the end points of the subinterval $\partial\Omega_i$ (see Fig. 5). The unknowns to be determined from this contribution to the boundary integral on the right-hand side of (33) are therefore n_1 approximations to ω at the midpoints of the subintervals $\partial\Omega_i$ and $n_1 + 1$ approximations to p at the end points of these subintervals. Clearly, the final term on the right-hand side of (47), involving only $\partial G_1/\partial n$ passes to the right-hand side of the system to be solved for the unknowns.

Along $C''D$ In a similar fashion, we write $C''D$ as the union of n_2 subintervals $\{\partial\Omega_i\}_{i=n_1+1}^{n_1+n_2}$ and again use the midpoint rule and central difference approximations to get

$$\begin{aligned}
&\int_{C''}^{D} \left(\frac{\partial \omega}{\partial n} G_2 - \omega \frac{\partial G_2}{\partial n} + \frac{\partial \psi}{\partial n} G_1 - \psi \frac{\partial G_1}{\partial n} \right) ds \\
&= \int_{C''}^{D} \left(\frac{\partial p}{\partial s} G_2 + \frac{\partial \psi}{\partial n} \left(2\kappa \frac{\partial G_2}{\partial n} + G_1 \right) - \frac{\partial G_1}{\partial n} \right) ds \\
&\approx \sum_{i=n_1+1}^{n_1+n_2} \left(\frac{p_{i+2} - p_{i+1}}{\Delta s_i} \right) \int\limits_{\partial\Omega_i} G_2 \, ds + \left(\frac{\partial \psi}{\partial n} \right)_i \int\limits_{\partial\Omega_i} \left(2\kappa \frac{\partial G_2}{\partial n} + G_1 \right) ds \; - \int\limits_{\partial\Omega_i} \frac{\partial G_1}{\partial n} \, ds,
\end{aligned} \tag{50}$$

where Δs_i denotes the arclength of the ith subinterval $\partial\Omega_i$. The unknowns to be determined from this contribution to the boundary integral are now, therefore, n_2 approximations to $\partial\psi/\partial n$ at the midpoints of the subintervals $\partial\Omega_i$ and $n_2 + 1$ approximations to p at the end points of these subintervals. As before, the final term on the right-hand side of (50), involving only $\partial G_1/\partial n$ passes to the right-hand side of the system to be solved for the unknowns.

Along EA The contribution along EA to the integral on the right-hand side of (33) is particularly simple due to the vanishing of both ω and ψ along the axis of symmetry. The decomposition of AE into n_3 subintervals $\{\partial\Omega_i\}_{i=n_1+n_2+1}^{n_1+n_2+n_3}$ and the use of the midpoint rule and central difference approximations leads to

$$\int_E^A \left(\frac{\partial p}{\partial s}G_2 + \frac{\partial \psi}{\partial n}G_1\right) ds \approx \sum_{i=n_1+n_2+1}^{n_1+n_2+n_3} -\left(\frac{p_{i+3}-p_{i+2}}{\Delta x_i}\right)\int_{\partial\Omega_i} G_2\, ds \; + \left(\frac{\partial \psi}{\partial n}\right)_i \int_{\partial\Omega_i} G_1\, ds, \tag{51}$$

where Δx_i denotes the length of $\partial\Omega_i$. The approximations to the pressure at the end points of the n_3 subintervals and the approximations to the normal derivative of the stream function at the midpoints of those subintervals represent the $(n_3+1+n_3 = 2n_3+1)$ unknowns to be found from this contribution to the boundary integral.

Along $C'C \cup CC''$ Along this portion of the boundary $\partial\Omega$ we use the singular forms (27) for p, (29) for ω and the normal derivative of (25) for $\partial\psi/\partial n$ and integration by parts for the integral of $\partial p/\partial s\; G_2$, as explained in Section 3.2. Thus we have

$$\begin{aligned}
&[pG_2]_{C'+}^{C''-} + \int_{C'}^{C}\left(-p\frac{\partial G_2}{\partial s} - \omega\frac{\partial G_2}{\partial n} - \frac{\partial G_1}{\partial n}\right) ds \\
&\qquad + \int_{C}^{C''}\left(-p\frac{\partial G_2}{\partial s} - \omega\frac{\partial G_2}{\partial n} + \frac{\partial \psi}{\partial n}G_1 - \frac{\partial G_1}{\partial n}\right) ds \\
&= [(C_1\Pi - c_p)G_2]_{C'+}^{C''-} + \int_{C'}^{C}\left(-(C_1\Pi - c_p)\frac{\partial G_2}{\partial s} - C_1\Omega\,\frac{\partial G_2}{\partial n} - \frac{\partial G_1}{\partial n}\right) ds \\
&\qquad + \int_{C}^{C''}\left(-(C_1\Pi - c_p)\frac{\partial G_2}{\partial s} - C_1\Omega\,\frac{\partial G_2}{\partial n} + C_1\Psi_n G_1 - \frac{\partial G_1}{\partial n}\right) ds \\
&= C_1\,[\Pi G_2]_{C'+}^{C''-} + \int_{C'}^{C}\left(-C_1\Pi\frac{\partial G_2}{\partial s} - C_1\Omega\,\frac{\partial G_2}{\partial n} - \frac{\partial G_1}{\partial n}\right) ds \\
&\qquad + \int_{C}^{C''}\left(-C_1\Pi\frac{\partial G_2}{\partial s} - C_1\Omega\,\frac{\partial G_2}{\partial n} + C_1\Psi_n G_1 - \frac{\partial G_1}{\partial n}\right) ds.
\end{aligned} \tag{52}$$

The sole unknown from this contribution to the boundary integral is the singular coefficient C_1 and, as along BC' and $C''D$, the terms on the right-hand side of (52) involving $\partial G_1/\partial n$ pass to the right-hand side of the system to be solved for the unknowns. Note that for simplicity the approximate form $y = \eta(x)$ was used in the evaluation of the integrals along CC'' since the difference between the graph of this function and that of the singular form (21) is very small, even if the curvature of the two curves at the separation point is very different (one finite, one infinite).

Summary of flow variables to be determined For a given free surface Γ the above paragraphs should make it clear that a total of $2(n_1+n_2+n_3)+4$ unknowns are to be calculated. To generate the same number of equations as unknowns we discretize, as explained above, eqns (32) and (33) with the choice of points (x', y') made equal to the Cartesian coordinates of the midpoints of the $n_1+n_2+n_3$ subintervals. This yields $2(n_1+n_2+n_3)$ equations. Assuming that the pressure is equal to that of the atmosphere at exit requires the prescription $p_{n_1+n_2+2} = p_{n_1+n_2+3} = 0$, supplying two more equations. The

assumption that at inflow fully developed conditions apply and that therefore the pressure is a constant along AB means that we should set $p_1 = p_{n_1+n_2+n_3+3}$, giving one more equation. Finally, we choose one other point $(x', y') \neq (0, 1)$ different from all the others and satisfy the discrete version of one of eqns (32) and (33) to complete the required number of equations and create a square and non-singular coefficient matrix for the system to be solved. As is usual with boundary integral methods this matrix is full but sufficiently small (even for the finest meshes used) that an efficient direct solver may be used.

3.2.2 Differences with the formulation of Hansen and Kelmanson [10], [11]
Comparing eqns (42) and (45) in addition to the respective discretizations employed by Hansen and Kelmanson [10], [11] and proposed in this article in Section 3.2.1 reveals a number of important differences between the two approaches:

1. The present formulation leads to a somewhat simpler expression than (42) by avoiding jump terms at the points C' and C''.
2. The present formulation avoids what may be very delicate evaluations of improper integrals of $p\partial G_1(x, y, x', y')/\partial s$ along paths passing through the point (x', y'). Instead, we may have improper integrals of $\partial p/\partial s G_1$, but all Cauchy principal values exist and are simple to evaluate. More specifically, if a subinterval $\partial\Omega_i$ consists of an arc segment of length Δs_i then, as explained in Section 3.2.1, we use central differences to write
$$\int_{\partial\Omega_i} \frac{\partial p}{\partial s} G_1(x, y, x', y')\, ds \approx \left(\frac{p_{i+1} - p_i}{\Delta s_i}\right) \int_{\partial\Omega_i} G_1(x, y, x', y')\, ds. \tag{53}$$
Let us denote the coordinates of the end points of $\partial\Omega_i$ by (x_i, y_i) and (x_{i+1}, y_{i+1}). Then, if $(x', y') \in \partial\Omega_i$ the Cauchy principal value of the integral appearing on the right-hand side of (53) is evaluated by expressing it as the sum of two convergent integrals: one over the subset of $\partial\Omega_i$ having end points (x_i, y_i) and (x', y') and the other over the subset of $\partial\Omega_i$ having end points (x', y') and (x_{i+1}, y_{i+1}). These are evaluated using an adaptive quadrature method: see Shampine [33].
3. When discretized (see Section 3.2.1) the new formulation will lead to a staggered boundary grid for the computation of p and ω along BC and of p and $\partial\psi/\partial n$ along $CD \cup EA$, the discrete pressure values being calculated at the end points of the subintervals $\{\partial\Omega_i\}_{i=1}^{n_1+n_2+n_3}$ and the remaining variables at the midpoints of these subintervals. This avoids possible problems with non-physical oscillatory pressure values or even pressure indeterminacy that may arise when all flow variables are collocated at the subinterval midpoints.

3.3 Determination of the free surface Γ

Thus far in the solution process, along $y = \eta(x)$ only the kinematic and shear-free conditions (13)–(15) have been satisfied and the free surface has been considered known. Of course, the correct free surface, along which the normal stress balance condition (17) is respected, must also be found. To find it we will use an iterative method and introduce the residual of the normal stress at $N + 1$ points along $C''D$, where we choose $N + 1 = 5n - 1$ in order to determine the parameters appearing in the linear combination (18) of the n basis functions η_i (see Section 2.3.1). We denote by R_i the residual of the normal stress balance at a point $(x_i, \eta(x_i))$ of the free surface:
$$R_i = p(x_i, \eta(x_i)) + 2\frac{\partial^2\psi}{\partial n \partial s}(x_i, \eta(x_i)) + \gamma\kappa(x_i, \eta(x_i)), \quad i = 1, 2, \ldots, N. \tag{54}$$

R_i is approximated numerically using simple central differences in the calculation of the approximative derivative with respect to arc length of $\partial\psi/\partial n$ and spline interpolation of this and the calculated approximation to the pressure.

Next we use the Levenberg–Marquardt [23], [24] method, implemented in `lsqnonlin` of MATLAB, to solve the non-linear least-squares problem

$$\min_{\boldsymbol{c}} \sum_{i=1}^{N+1} R_i^2(\boldsymbol{c}), \tag{55}$$

where $\boldsymbol{c}$ is the vector containing the $5n-1$ parameters appearing in the linear combination (18) of the n basis functions η_i. Once the minimum has been found we recalculate C_1 and all the flow variables as detailed in Section 3.2.1 and continue until $\boldsymbol{c}^{(k+1)}$, the $(k+1)$th iterative value of $\boldsymbol{c}$, satisfies some convergence criterion, such as

$$\|\boldsymbol{c}^{(k+1)} - \boldsymbol{c}^{(k)}\|_2 < s\,\|1 + \boldsymbol{c}^{(k)}\|_2, \tag{56}$$

for some suitably small choice of the relative step tolerance s. Numerical continuation may be used to obtain solutions on increasingly refined meshes. That is to say, the converged vector $\boldsymbol{c}$ calculated for a certain choice of n_1, n_2 and n_3 may be used to calculate the initial free surface shape when finer meshes are employed.

4 NUMERICAL RESULTS

Calculations were performed for values of the dimensionless surface tension $\gamma = 0.001$, 0.01, 0.1 and 1 on meshes where the total number M of boundary elements $\partial\Omega_i$ varied from $M = 1434$ (2872 unknowns) to $M = 1854$ (3712 unknowns). The radius r_c of the singular sector $\mathcal{W} \cap \overline{\Omega}$ was set equal to 10^{-5}. With the choice of $n = 10$ basis functions η_i (see (19)) the number of points $N+1$ where the normal stress balance residual (54) was evaluated was equal to $5n - 1 = 49$. The Levenberg–Marquardt algorithm (see Section 3.3) was considered to have converged when the inequality (56) was satisfied with a relative step tolerance $s = 10^{-6}$. It was found that this choice of s always ensured that the final value of the objective function (55) was no more than $O(10^{-5})$.

4.1 Shape of the free surface

In Figs 6 to 8 we plot the converged free surface function $y = \eta(x)$, given by the linear combination (18), in addition to its first and second derivatives, over the full range of dimensionless surface tensions. It may be observed from Figs 7 and 8 that, for any given surface tension γ, the (positive) slope of the free surface attains a maximum at some point $0 < x_\gamma \ll 1$ and that the second derivative grows dramatically as $x \to 0$. These results were computed on the finest mesh ($M = 1854$) and in Section 3.3 we have explained how the parameters $\{\alpha_i, \varepsilon_{\infty,i}, \varepsilon_{0,i}, \gamma_i\}$ were calculated. Once they have been found it remains the case, however, that

$$\eta''(0) = -2\sum_{i=1}^{n} \beta_i\alpha_i(\epsilon_{0,i} - \epsilon_{\infty,i})\gamma_i,$$

is finite and that there is no reason to expect that

$$\eta'(0) = \sum_{i=1}^{n} \beta_i\alpha_i\epsilon_{0,i},$$

will equal $\tan(\alpha)$.

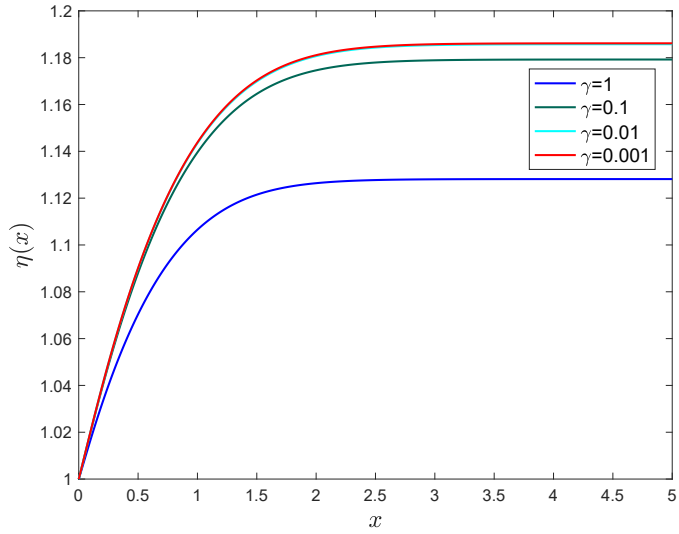

Figure 6: $n_1 = n_2 = n_3 = 618$. Free surface $y = \eta(x)$ computed at values 1, 0.1, 0.01 and 0.001 of the dimensionless surface tension γ.

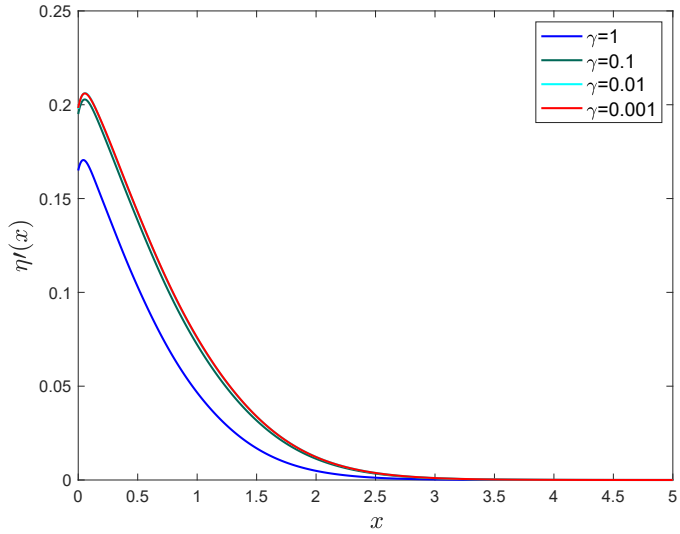

Figure 7: $n_1 = n_2 = n_3 = 618$. First derivative $y = \eta'(x)$ computed at values 1, 0.1, 0.01 and 0.001 of the dimensionless surface tension γ.

Given the deficiencies noted above of the representation (18) of the free surface in a neighbourhood of the separation point, we match the correct leading order asymptotic form (21), as explained in Section 2.3.2, to this far-field solution. In Fig. 9 we show the results of the matching at $x = x_0$ of (18) with (21), as computed on the $M = 1854$ mesh. Over

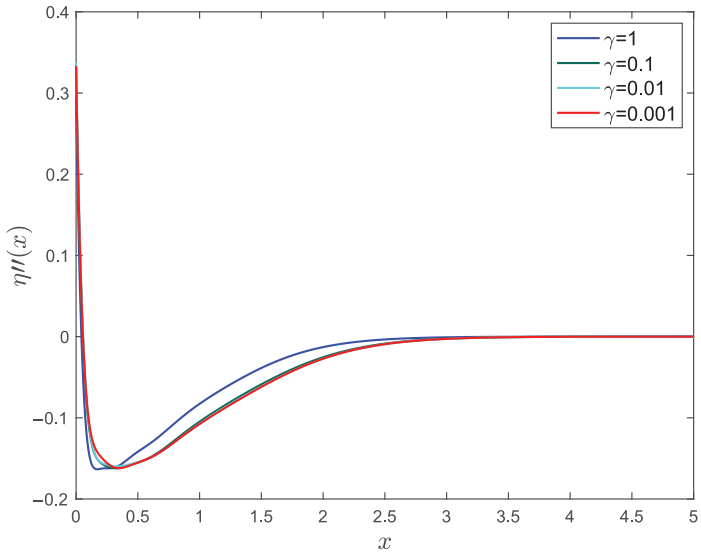

Figure 8: $n_1 = n_2 = n_3 = 618$. Second derivative $y = \eta''(x)$ computed at values 1, 0.1, 0.01 and 0.001 of the dimensionless surface tension γ.

$x \in [0, 2r_c]$ the graphs of (18) and (21) shown in Fig. 9 appear to the naked eye to be those of linear functions. In reality, $\kappa(0)$, the curvature at the origin, is infinite.

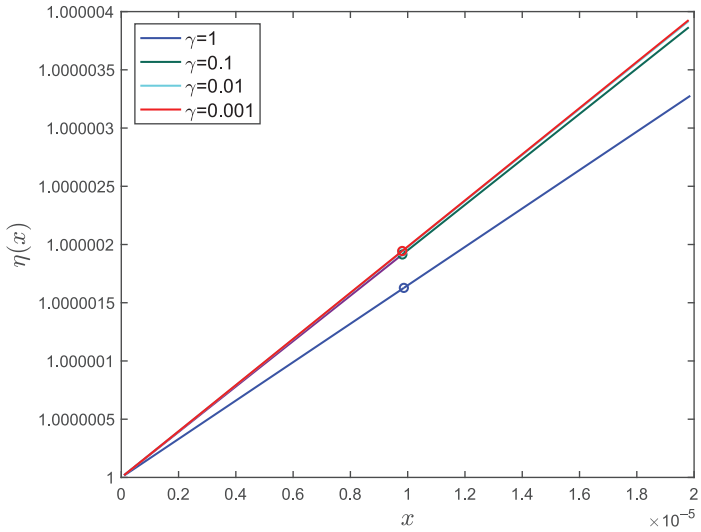

Figure 9: $n_1 = n_2 = n_3 = 618$. Matching of the inner solution $y = 1 + h(r)$ (21) to the outer solution $y = \eta(x)$ (18) at $x = x_0$ (see (31)) at values 1, 0.1, 0.01 and 0.001 of the dimensionless surface tension γ.

4.2 Extrudate swell ratio η_∞

Comparison of the calculated values of η_∞ on meshes with $M = 1434$, 1644 and 1854 is made in Table 1 with the results of the original boundary element method calculations with $M = 1854$ of Owens [14], with the result (at $\gamma = 1$) of the high-resolution finite element method of Salamon et al. [17], and with some of the results of the singular finite element calculations of Georgiou and Boudouvis [25] and of the finite element method of Mitsoulis et al. [19]. Since the result of Salamon et al. [17] was computed on a highly refined finite element mesh involving 171258 unknowns we believe that this may be considered to be a benchmark value for the case $\gamma = 1$. The value of the extrudate swell ratio at this value of γ computed by Georgiou and Boudouvis [25] is within 0.026% of the benchmark value and was obtained on a finite element mesh having 30866 unknowns. The results of Mitsoulis et al. [19] were obtained using meshes having either 22548 or 30866 degrees of freedom. Our calculation of η_∞ at $\gamma = 1$ using the $M = 1854$ boundary integral mesh is within 0.0629% of the value of Salamon et al. but was obtained using a mesh having only 3712 degrees of freedom. In this example, the cost advantages of using a boundary element method are clear. From the evidence presented in Table 1 it would seem that slightly higher values of η_∞ might be expected were we able to compute results on yet finer meshes, bringing them into even closer agreement with the results of Georgiou and Boudouvis [25], Mitsoulis et al. [19] and Salamon et al. [17]. Regrettably, however, calculations for $M > 1854$ are beyond what we can perform conveniently with the computing resources currently at our disposal.

Table 1: Values of the extrudate swell ratio η_∞ for different values of the non-dimensional surface tension γ, computed using the boundary integral equation method and M boundary elements.

γ	Present method			Owens [14]	Georgiou and Boudouvis [25]	Mitsoulis et al. [19]	Salamon et al. [17]
	M=1434	M=1644	M=1854				
1	1.1279	1.1280	1.1281	1.1282	1.1291	1.129	1.12881
10^{-1}	1.1784	1.1793	1.1792	1.1792	1.1794	1.180	-
10^{-2}	1.1853	1.1853	1.1858	1.1857	-	1.186	-
10^{-3}	1.1859	1.1861	1.1861	1.1861	-	-	-
10^{-5}	-	-	-	-	-	1.186	-

4.3 Separation angles and leading order indices

In Table 2 we show the values of the parameters α (in radians and degrees) and λ_1 computed on the finest mesh and compare these with the results obtained by Owens [14] using a boundary integral method. We note in Table 2 a few very minor differences between the parameter values attributed to Owens [14] and those in his original article. This is because of small errors found in the calculation of the parameters A_2, B_2, C_2 and D_2 appearing in (23) since the article of Owens went to press. Agreement between our results and those of Owens [14] is excellent although the present results should be viewed as the more accurate of the two sets.

In the second and third columns of Table 2 we display the results for the separation angles in both radians and degrees when $\gamma = 1, 0.1, 0.01$ and 0.001, as computed on the finest mesh.

Following the ansatz by Schultz and Gervasio [16] for the form of the free surface $y = \eta(x)$ near the separation point:

$$\eta(x) - 1 = a + bx + cx^n, \tag{57}$$

for certain parameters a, b, c and n, Salamon et al. [17] estimated b to be equal to 0.176 when $\gamma = 1$ and $Re = 0$. Comparing (57) with (21) and noting that $r \approx x/\cos(\alpha - \pi)$ we can therefore estimate, when $\gamma = 1$, $\alpha \approx (180 + \arctan(0.176)) = 189.98°$, which is in satisfactory agreement with our own result of $189.37°$. Experimental results reported by Nickell et al. [26], Tanner [27] and Tanner et al. [28] were all for Reynolds numbers below 10^{-3} and those of Batchelor et al. [29] were for $Re \approx 10^{-8}$. The data from the experimental results reported by these authors showed separation angles to be between $189°$ and $194°$, so that our calculated values of α are well within the range of those measured experimentally.

There are very few results available in the literature for the index λ_1. Salamon et al. [17] estimated the value of the parameter n in the ansatz (57) to be 1.43 when $\gamma = 1$ and $Re = 0$, so that again, comparing (57) with (21) gives $\lambda_1 = n - 1 = 0.43$, not too far from the computed value shown in the first row and fourth column of Table 2.

Table 2: Values of the parameters α and λ_1 appearing in (21). The far-field solutions were computed on the finest mesh ($M = 1854$).

	Present method			Owens [14]†	
γ	α (radians)	α (degrees)	λ_1	α (radians)	λ_1
1	3.3051	189.3667	4.5317×10^{-1}	3.3049	4.5321×10^{-1}
10^{-1}	3.3342	191.0373	4.4587×10^{-1}	3.3337	4.4599×10^{-1}
10^{-2}	3.3368	191.1872	4.4522×10^{-1}	3.3363	4.4535×10^{-1}
10^{-3}	3.3371	191.2032	4.4516×10^{-1}	3.3363	4.4536×10^{-1}

† Results corrected since the publication of Owens [14].

5 CONCLUSIONS

In the present paper we have presented a new BIM which is suitable for free surface boundary value problems involving creeping flows of a viscous fluid. The method has been applied to the problem of the planar extrusion of such a fluid. It has been pointed out in the Introduction that because the shape of the free surface is typically non-trivial and unknown a priori so-called singularity annihilation BIMs (see, for example, Kelmanson and Lonsdale [7]) are unusable, and that it is also impossible to employ singularity subtraction BIMs in such a way that the transformed variables have the required regularity properties throughout the flow domain.

The new BIM proposed in this article builds upon an existing idea of Hansen and Kelmanson [10], [11] which uses the change of variable (37) and integration by parts to perform the boundary integral along paths that pass through a singularity where $\partial\omega/\partial n$ may not be integrable but p is. We do the same. The essential difference between our formulation and that of Hansen and Kelmanson is in the treatment of the integration of $\partial p/\partial s G_j$ $(j = 1, 2)$ in subintervals $\partial\Omega_i$ $(i = 1, 2, \ldots, n_1 + n_2 + n_3)$ some distance from the singularity. It has been seen in Section 3.2.2 to be advantageous in such boundary elements to evaluate numerically the integral of $\partial p/\partial s G_j$ without performing an integration by parts. The result is a staggered boundary grid for the computation of p and the other flow variables.

The new BIM also has the advantage over the earlier work of Owens [14] in that we integrate around the true boundary of the flow domain whereas, due to the non-integrability

of $\partial\omega/\partial n$ at the point of separation, Owens [14] skirted around this singular point following a circular arc, introducing an error, even though the radius of the arc centred at the separation point was small and the correct singular representations of the variables were employed along it.

The results shown in Section 4.2 for the extrudate swell ratio over a range of capillary numbers are in excellent agreement with others in the numerical literature [14], [17], [19], [25]. However, the extrudate swell ratio is a somewhat crude measure of the correctness of the solution. Therefore, in Section 4.3 we also post our calculated values for the separation angles α and leading order indices λ_1 appearing in the asymptotic form of the flow variables in the immediate neighbourhood of the separation point. Here there is a dire shortage of data in the literature with which we can compare our results although where theoretical [16], numerical [17] and experimental [26]–[29] results have been previously published agreement would appear to be convincing.

ACKNOWLEDGMENTS

The authors wish to thank Mark Kelmanson for pointing us to the references by Hansen and Kelmanson [10], [11] . We acknowledge the support of the Natural Sciences and Engineering Research Council of Canada (NSERC). Cette recherche a été financée par le Conseil de recherches en sciences naturelles et en génie du Canada (CRSNG).

REFERENCES

[1] Kelmanson, M.A., Modified integral equation solution of viscous flows near sharp corners. *Computers and Fluids*, **11**, pp. 307–324, 1983.
[2] Kelmanson, M.A., An integral equation method for the solution of singular slow flow problems. *J. Comput. Phys.*, **51**, pp. 139–158, 1983.
[3] Symm, G.T., Treatment of singularities in the solution of Laplace's equation by an integral equation method. Report NAC31, National Physical Laboratory, Teddington, UK, 1973.
[4] Ingham, D.B. & Kelmanson, M.A., A note on the comparison between BIE and FD techniques for solving elliptic BVPs with boundary singularities. *Commun. Appl. Numer. Methods*, **2**, pp. 189–193, 1986.
[5] Kelmanson, M.A., Solution of nonlinear elliptic equations with boundary singularities by an integral method. *J. Comput. Phys.*, **56**, pp. 244–258, 1984.
[6] Ingham, D.B. & Kelmanson, M.A., Solution of nonlinear elliptic equations with boundary singularities by an integral method. *Boundary Integral Equation Analyses of Singular, Potential and Biharmonic Problems*, eds C.A. Brebbia & S.A. Orszag, Springer Verlag, vol. 7 of *Lecture Notes in Engineering*, pp. 89–113, 1984.
[7] Kelmanson, M.A. & Lonsdale, B., Annihilation of boundary singularities via suitable Green's functions. *Computers Math. Applic.*, **29**, pp. 1–7, 1995.
[8] Moffatt, H.K., Viscous and resistive eddies near a sharp corner. *J. Fluid Mech.*, **18**, pp. 1–18, 1964.
[9] Karageorghis, A. & Fairweather, G., The method of fundamental solutions for the numerical solution of the biharmonic equation. *J. Comput. Phys.*, **69**, pp. 434–459, 1987.
[10] Hansen, E.B. & Kelmanson, M.A., Integral equation analysis of the driven-cavity boundary singularity. *Appl. Math. Lett.*, **5**, pp. 15–19, 1992.
[11] Hansen, E.B. & Kelmanson, M.A., An integral equation justification of the boundary conditions of the driven-cavity problem. *Computers and Fluids*, **23**, pp. 225–240, 1994.

[12] Xu, B., Some Problems in Slow Viscous Flow. PhD thesis, Danish Centre for Applied Mathematics and Mechanics, Lyngby, Denmark, 1985.
[13] Michael, D.H., The separation of a viscous liquid at a straight edge. *Mathematika*, **5**, pp. 82–84, 1958.
[14] Owens, R.G., The separation angle of the free surface of a viscous fluid at a straight edge. *J. Fluid Mech.*, **942**, pp. A50–1–A50–31, 2022.
[15] Anderson, D.M. & Davis, S.H., Two-fluid viscous flow in a corner. *J. Fluid Mech.*, **257**, pp. 1–31, 1993.
[16] Schultz, W.W. & Gervasio, C., A study of the singularity in the die-swell problem. *Q. J. Mech. Appl. Math.*, **43**, pp. 407–425, 1990.
[17] Salamon, T.R., Bornside, D.E., Armstrong, R.C. & Brown, R.A., The role of surface tension in the dominant balance in the die swell singularity. *Phys. Fluids*, **7**, pp. 2328–2344, 1995.
[18] Kelmanson, M.A., Boundary integral equation solution of viscous flows with free surfaces. *J. Engrg. Math.*, **17**, pp. 329–343, 1983.
[19] Mitsoulis, E., Georgiou, G.C. & Kountouriotis, Z., A study of various factors affecting Newtonian extrudate swell. *Computers and Fluids*, **57**, pp. 195–207, 2012.
[20] Ramalingam, S., Fiber Spinning and Rheology of Liquid-Crystalline Polymers. PhD thesis, Massachusetts Institute of Technology, Cambridge, MA, USA, 1994.
[21] Burda, P., On the FEM for the Navier–Stokes equations in domains with corner singularities. *Finite Element Methods, Superconvergence, Post-Processing and A Posteriori Estimates*, eds M. Křížek, P. Neittaanmäki & R. Stenberg, Marcel Dekker: New York, pp. 41–52, 1998.
[22] Lugt, H.J. & Schwiderski, E.W., Flows around dihedral angles, I: Eigenmotion analysis. *Proc. Roy. Soc. A*, **285**, pp. 382–399, 1965.
[23] Levenberg, K., A method for the solution of certain problems in least squares. *Quart. Appl. Math.*, **2**, pp. 164–168, 1944.
[24] Marquardt, D.W., An algorithm for least-squares estimation of nonlinear parameters. *SIAM J. Appl. Math.*, **11**, pp. 431–441, 1963.
[25] Georgiou, G.C. & Boudouvis, A.C., Converged solutions of the Newtonian extrudate-swell problem. *Int. J. Numer. Meth. Fluids*, **29**, pp. 363–371, 1999.
[26] Nickell, R.E., Tanner, R.I. & Caswell, B., The solution of viscous incompressible jet and free-surface flows using finite-element methods. *J. Fluid Mech.*, **65**, pp. 189–206, 1974.
[27] Tanner, R.I., Separation of viscous jets using boundary element methods. *Proceedings of the 9th Australasian Fluid Mechanics Conference*, University of Auckland School of Engineering: Auckland, New Zealand, pp. 247–250, 1986.
[28] Tanner, R.I., Lam, H. & Bush, M.B., The separation of viscous jets. *Phys. Fluids*, **28**, pp. 23–25, 1985.
[29] Batchelor, J., Berry, J.P. & Horsfall, F., Die swell in elastic and viscous fluids. *Polymer*, **14**, pp. 297–299, 1973.
[30] Batchelor, G.K., *An Introduction to Fluid Dynamics*. Cambridge University Press: Cambridge, UK, 1967.
[31] Longuet-Higgins, M.S., Mass transport in water waves. *Proc. R. Soc. Lond. A*, **245**, pp. 535–581, 1953.
[32] Sturges, L.D., Die swell: The separation of the free surface. *J. Non-Newtonian Fluid Mech.*, **6**, pp. 155–159, 1979.
[33] Shampine, L., Vectorized adaptive quadrature in MATLAB. *J. Comput. Appl. Math.*, **211**, pp. 131–140, 2008.